

Validating Multipath Responses of Moving Targets Through Urban Environments

Robert Linnehan

Air Force Research Laboratory, Sensors Directorate
Hanscom AFB, MA, 01731

Email: robert.linnehan@us.af.mil; Telephone: (781)377-9842

John Schindler

Solid State Scientific Corporation
Hanscom AFB, MA 01731

Email: j.schindler@ieee.org; Telephone: (781)377-1732

Abstract—This work proceeds from the paper we published in RadarCon 2009 titled “Multistatic scattering from moving targets in multipath environments”, where we explored the potential to track moving ground targets with radar as they enter urban areas and become obscured by buildings. An X-band radar data collection was performed which validates the predicted multipath response, and the received multipath power in relation to the line-of-sight (LOS) response. Results from a bistatic experiment are used to examine the spatial coherency of energy reflecting from a large, rough surface, and the power distribution in angle that illuminates a target as it traverses in front of a building. This experiment may inspire knowledge-based methods to coherently process multipath returns, beyond that of standard GMTI processing, i.e., free-space matched-filtering (FFT) and CFAR detection.

I. INTRODUCTION

In [1] we modeled the radar response of a target moving through an urban canyon, including interactions with the background wall and the multipath relation to the line-of-sight (LOS) response. The two-dimensional analysis included near-field reradiation from the illuminated wall to a target having a multistatic response, i.e., a target that scatters some portion of energy in all directions. We also evaluated the degradation of power and coherency in the signal processing attributed to surface roughness of the reflecting wall.

The work was in support of DARPA’s *Multipath Exploitation Radar* (MER) program that proposes to track moving ground targets with airborne radar, even as LOS paths are obstructed by buildings and other large structures when targets enter urban centers [2]. If knowledge of the urban geometry is available, energy reflected from building walls down to moving vehicles in the street, and returning on the reciprocal paths could be utilized to improve the detection rate and maintaining track. This will ultimately reduce the number of airborne platforms required to adequately sustain GMTI radar coverage over a city or town.

In August 2009 we performed a controlled, outdoor experiment using a Lintek élan 2000 radar system to collect X-band data. The experiment consisted of a bistatic collection to characterize the reradiation of an illuminated building, as well as a monostatic collection where vehicles passed in front of the wall to yield both LOS and multipath data. A site at Wright-Patterson AFB was selected with an open parking area that faced an isolated two-story brick building of sufficient

length. The building face is flat and fairly innocuous in terms of its structure, having two rows of windows, several down spouts, a metal door and a concrete staircase at one end. The parking area was restricted during the test so no vehicles, stationary or moving, would interfere with the collection. The only obstruction was a metal light pole positioned to the right side of the transmit beam.

The basic geometry for the experiment is shown in the two-dimension diagram (overhead view) in Figure 1. The building is 54 m in length and 12 m in height, and was illuminated in the far-field using two sectoral horn antennas (to transmit both horizontal and vertical polarized fields) located 42.7 m from the right corner. The transmitters were oriented so their mainbeams were narrow in elevation (12 degrees) and wide in azimuth (55 degrees). The center of the transmit mainbeams were directed toward the center of the building yielding a 40 degree incident angle with the reflecting surface. Most of the transmit energy was utilized since the mainbeams primarily encompassed only the facing wall. Two absorber fences were placed 5 m and 10 m in front of the transmitters in order to mitigate the ground bounce and help to isolate the multipath. A photograph of the building, as seen from the transmitters, is shown in Figure 2.

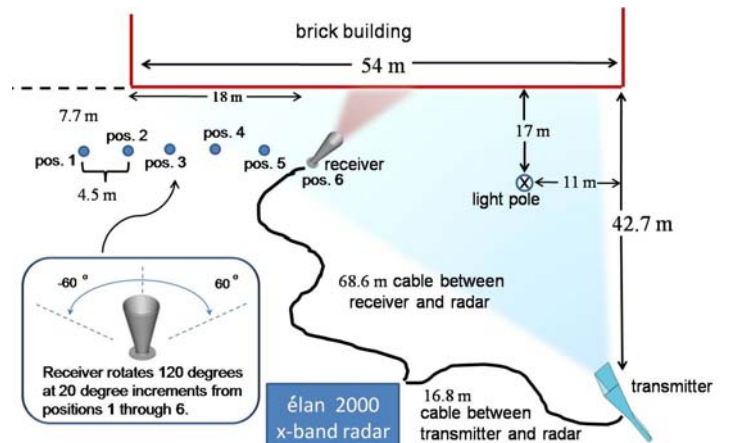


Fig. 1. Overhead geometry of the bistatic radar collection.

Report Documentation Page			Form Approved OMB No. 0704-0188	
<p>Public reporting burden for the collection of information is estimated to average 1 hour per response, including the time for reviewing instructions, searching existing data sources, gathering and maintaining the data needed, and completing and reviewing the collection of information. Send comments regarding this burden estimate or any other aspect of this collection of information, including suggestions for reducing this burden, to Washington Headquarters Services, Directorate for Information Operations and Reports, 1215 Jefferson Davis Highway, Suite 1204, Arlington VA 22202-4302. Respondents should be aware that notwithstanding any other provision of law, no person shall be subject to a penalty for failing to comply with a collection of information if it does not display a currently valid OMB control number.</p>				
1. REPORT DATE MAY 2010	2. REPORT TYPE	3. DATES COVERED 00-00-2010 to 00-00-2010		
4. TITLE AND SUBTITLE Validating Multipath Responses of Moving Targets Through Urban Environments			5a. CONTRACT NUMBER	
			5b. GRANT NUMBER	
			5c. PROGRAM ELEMENT NUMBER	
6. AUTHOR(S)			5d. PROJECT NUMBER	
			5e. TASK NUMBER	
			5f. WORK UNIT NUMBER	
7. PERFORMING ORGANIZATION NAME(S) AND ADDRESS(ES) Air Force Research Laboratory, Sensors Directorate, Hanscom AFB, MA, 01731			8. PERFORMING ORGANIZATION REPORT NUMBER	
9. SPONSORING/MONITORING AGENCY NAME(S) AND ADDRESS(ES)			10. SPONSOR/MONITOR'S ACRONYM(S)	
			11. SPONSOR/MONITOR'S REPORT NUMBER(S)	
12. DISTRIBUTION/AVAILABILITY STATEMENT Approved for public release; distribution unlimited				
13. SUPPLEMENTARY NOTES See also ADM002322. Presented at the 2010 IEEE International Radar Conference (9th) Held in Arlington, Virginia on 10-14 May 2010. Sponsored in part by the Navy.				
14. ABSTRACT <p>This work proceeds from the paper we published in RadarCon 2009 titled ?Multistatic scattering from moving targets in multipath environments?, where we explored the potential to track moving ground targets with radar as they enter urban areas and become obscured by buildings. An X-band radar data collection was performed which validates the predicted multipath response, and the received multipath power in relation to the line-of-sight (LOS) response. Results from a bistatic experiment are used to examine the spatial coherency of energy reflecting from a large, rough surface, and the power distribution in angle that illuminates a target as it traverses in front of a building. This experiment may inspire knowledge-based methods to coherently process multipath returns, beyond that of standard GMTI processing, i.e., free-space matched-filtering (FFT) and CFAR detection.</p>				
15. SUBJECT TERMS				
16. SECURITY CLASSIFICATION OF:			17. LIMITATION OF ABSTRACT Same as Report (SAR)	18. NUMBER OF PAGES 6
a. REPORT unclassified	b. ABSTRACT unclassified	c. THIS PAGE unclassified	19a. NAME OF RESPONSIBLE PERSON	



Fig. 2. The reflecting wall as seen from the transmitter. Absorber fences are positioned to mitigate ground bounce interference. The light pole intercepts some energy on the right side on the transmit beam.

The data collection consisted of three portions that we describe with detail in the sections to follow. First of all, bistatic measurements were collected in order to determine the near-field power distributed onto a target from a reradiating wall that is illuminated in the far-field by an X-band radar. The “target” in this case was a conical horn antenna placed in the street in front of the building. The mainbeam of the receive antenna was physically steered and repositioned to isolate the response of the wall. Another bistatic experiment was performed to determine the spatial coherency of subsequent multipath pulses incident on a moving target. Finally, a monostatic radar collection of moving vehicles allowed us to compare multipath responses to corresponding direct path (LOS) responses.

II. POWER DISTRIBUTION FROM A RERADIATING BRICK BUILDING

For the primary bistatic measurements, a conical horn antenna was used as the receiver and was placed in the near-field of the building with the mainbeam directed toward the reflecting wall. The building is in the far-field region of the receiver. The transmit antennas remained stationary throughout the experiment. The receive antenna was secured to a tripod and placed on a cart that could be easily moved to the six bistatic positions, identified in Figure 1, along a line parallel to the wall. At each of these positions the receiver rotated between -60° and 60° in 20° increments on the tripod axis (with 0° being normal to the wall). For every receiver position and antenna angle, a step-frequency pulse centered at 10 GHz over a 3.5 GHz bandwidth was transmitted in discrete steps of 5 MHz (700 samples per transmission). Both the HH and VV polarized waveforms were collected by changing cables between the transmit antennas described in section I.

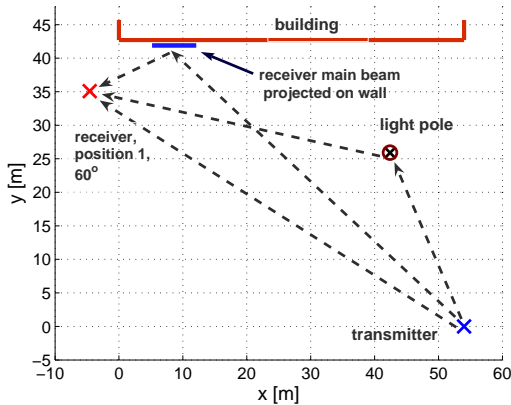
The purpose of the bistatic measurements is to gain an understanding of the physics associated with electromagnetic fields that propagate to a large, rough surface and reradiate

energy toward a ground target. A radar system designed to track vehicles in urban environments by utilizing multipath can only perform as well as the ability to correctly make detections for some nearly sequential coherent processing intervals (CPI) while the target is obscured. Accurate knowledge of the urban landscape is needed for tracking since non-LOS paths the electromagnetic energy traverses will modify the target’s position in space and Doppler. However, it is less apparent that knowledge of the city’s geometry may also be required to harness enough multipath energy to detect moving targets in the first place.

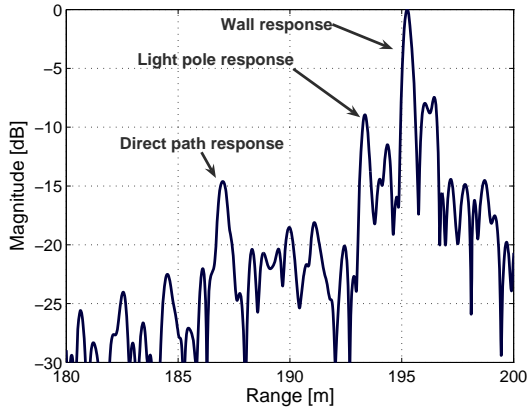
The output of the radar is the mixed and low-pass filtered complex signals. We begin by examining one of the waveforms to verify that our geometrical model is consistent with the measurements. This was a vertically polarized pulse on transmit that was collected from position 1 with the receive antenna at 60° . The geometry for this collection is illustrated in Figure 3(a), where the x and y dimensions are labeled on the axes. The z dimension is not shown in the diagram but note that the transmitter and receiver are 0.74 m and 2.06 m above the ground, respectively, and the light pole extends in elevation through the transmitter main beam. Pulse compression was performed on the measured data and the magnitude of the range profile, normalized to its peak value, is plotted in Figure 3(b). A simple electromagnetic modeling method, employing ray-tracing and point scatterers, was used to create a model of the range profile from this receiver configuration and is plotted in Figure 3(c), also normalized to the peak magnitude. The purpose of this comparison is to verify that delays from artifacts in the scene match reasonably well with the model, and allows us to confirm the region of each range profile that can be attributed to the wall reflection. This verification process was performed for the data collected from all six receive positions.

The conical horn receive antenna is 13 cm in diameter and thus has a beam width of approximately 11° . Projecting the receive beam onto the wall and accounting for skewness when the incident angle is oblique, we can predict the portion of the range profile that is bounded by the bistatic ellipse. The ellipse is defined by the transmitter and receiver locations, and their relation to the building. This allows us to isolate the power reflected from the wall to a near-field position, based on the predicted -3 dB edges of the receiver’s radiation pattern projected onto the wall. Verifying the location of the wall response when it is large, such as at 60° in Figure 3, is important because the responses are much weaker when the antenna is directed away from the reflected beam, i.e., when the receive angles are negative.

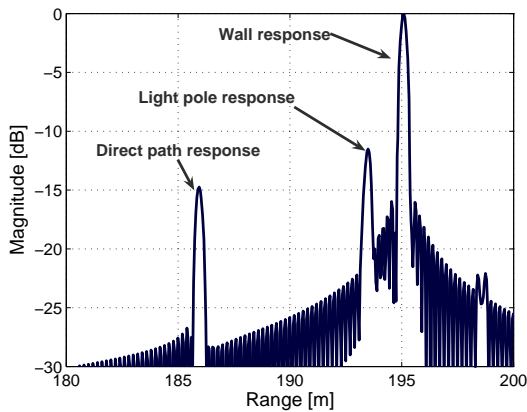
Distributions of the wall response power for both polarizations are shown as an intensity images in Figure 4. The power is displayed as function of the receive antenna position and angle. Note that for both polarizations, the power received from the wall is strongest when the antenna is at 40° or 60° for all positions. This is to be expected since the receive horn is pointing near the angle of reflection for the transmit field in these cases, i.e., the receiver is close to the specular angle.



(a) Geometry for data collected at position 1, angle 60°.



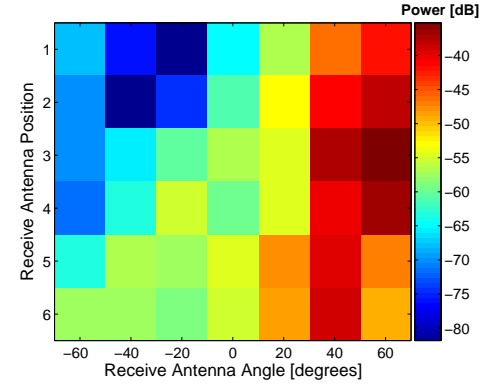
(b) Range profile for data collected at position 1, angle 60°.



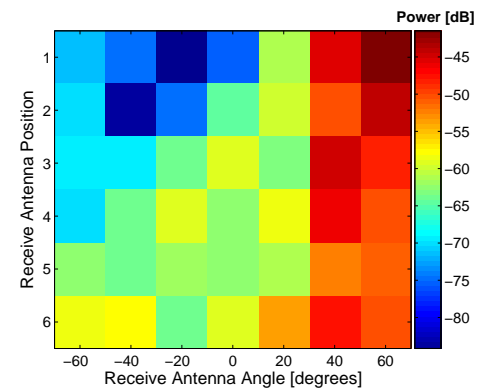
(c) Model range profile for position 1, angle +60°.

Fig. 3. Comparing real data with our geometric model of the scene.

The pertinent information to glean from this experiment is



(a) Vertical polarization.



(b) Horizontal polarization.

Fig. 4. Power due to the wall response for a given receiver position and angle.

that some amount of radiation propagates to the target from the entire wall. This is illustrated by examining the top, left corners of the intensity plots in Figures 4(a) and 4(b), where the receive antenna is pointing away from the transmitter and beyond the end of the building. Here the received power is 35 to 45 dB below the strongest return. The bottom, left corners in the intensity plots, where the receiver horn is pointed away from the receiver but still illuminates the reflecting wall, exhibit stronger responses between 15 to 25 dB below the peak returns. The trends here are consistent with our near-field integration modeling method in [1], and may lead to knowledge-based detection methods that harness energy other than that expected in the specular region of a target.

III. SPATIAL COHERENCY OF MULTIPATH SIGNALS

A secondary bistatic experiment took place with the receiver initially located at position 4 identified in Figure 1. Here the antenna was slowly rotated on its axis toward the wall, while the transmitter emitted a continuous signal to empirically determine the angle that maximized the received power, i.e., the specular angle in relation to the transmitter. We found

the specular angle to be 55° and maintained that orientation while the entire receiver assembly (tripod and antenna) was translated in sub-wavelength increments along a line parallel with the wall. The assembly was moved in the positive x direction up to 20 cm away from the original location. Data was collected for both polarizations in 1 cm ($\lambda/3$) increments in order to characterize the spatial coherency of X-band fields reflected from a rough surface, i.e., the windowed, brick wall.

We modeled this experiment assuming reflections occur from the specular point on the wall between the transmit and receive antennas. Using notation consistent with [1], the received signal model is

$$e_{1\text{way}}(u, k) = \frac{1}{r_1(u) \cdot r_2(u)} e^{-j2\pi f_k/c[r_1(u) + r_2(u)]}, \quad (1)$$

where f_k is the k^{th} frequency sample of the step-frequency pulse, c is the speed of light, r_1 is the range from the transmit antenna to the wall, r_2 is the range from the wall to the receive antenna, and u is the pulse index.

We want examine the phase variation of the data after the pulses are compressed. Since the specular angle was manually determined by rotating the receive antenna we are assured that the dominant scattering is due to the wall. For every transmit signal u , the pulse compressed data is

$$\Psi_u(r) = \sum_{k=1}^K w_k^*(r) \cdot e_{1\text{way}}(u, k), \quad (2)$$

where K is the total number of frequency samples (in this case 700) and $w_k^*(r)$ are the complex weights that depend on range r . From the geometry we know that the wall response should occur around 185 m in the range profile given the receiver is at position 4 (including the delay through the cable). Therefore r varies between 170 m 190 m at a sampling rate of 46.6 samples/meter, equivalent to a sample every $0.5 \cdot \delta_r$, where $\delta_r = 4.3$ cm is the range resolution.

The operation in (4) was performed on both the model signal and the horizontally polarized measured data. Figure 5 shows the phase angle of the maximum sample in the range profile magnitude. If we define

$$\phi_u = \angle [\max_r \{|\Psi_u(r)|\}], \quad (3)$$

then we are plotting ϕ_u for both the model and the measurement. The green “-.” curve in Figure 5 is fully sampled in space (over the antenna translation from 0 to 20 cm) to show the ideal phase angle response. The solid blue curve shows the phase angle response of the model with the same spatial sampling as that of the measurements. Comparing the ideal model to the sparsely sampled model shows the 1 cm spacing between samples yields errors in the peaks of the curve, but the negative slopes of the curve, as the phase varies from its maximum to minimum, are aligned with the ideal curve. The measured phase angle variation is displayed as the red “-” curve. Notice that the first few cycles of the experimental data is well aligned with the model, but the error begins to noticeably increase after the 8 cm mark on the abscissa. Here

the slopes of the measured data differ slightly from the model phase angle and the error accumulates through the end of the receiver translation.

One factor contributing to the phase angle error is the limited precision of the spatial measurements. The receiver assembly was place on a large cart that had to be manually shifted in 1 cm increments across the blacktop surface. Although the cart was well designed to move in small intervals and we took care to maintain proper orientation with every adjustment, it is inevitable that some amount of non-uniformity among the spacings could manifest in phase angle inaccuracies in the pulse compressed data. Another factor contributing to the phase angle error could be the extraneous features of the building. For instance, the down spouts or windows may be influencing the signal beyond the 8 cm mark. (We cannot identify the true specular point on the building in the post-experimental analysis to notice if these features intercept the center of the receiver mainbeam). Finally, the roughness of the reflecting surface (bricks and mortar) could also result in small phase variations in the measurements that carry over to the pulse compressed data.

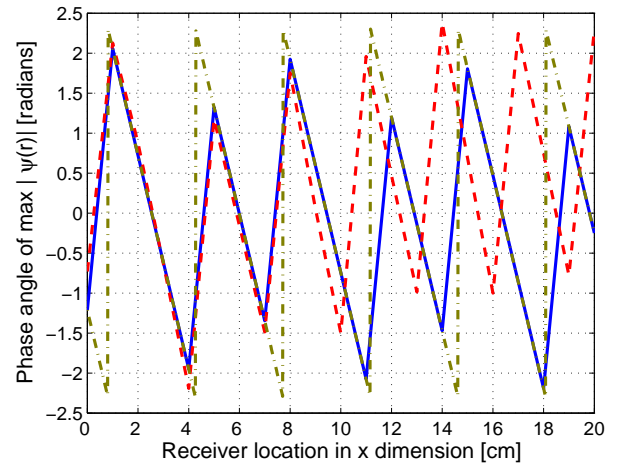


Fig. 5. Phase angle of the wall response (after pulse compression) as the receiver shifts from position 4 (at 0 cm) in the $+x$ direction in 1 cm steps up to 20 cm from position 4. The measured phase angle is represented by the dashed line in red, the model phase angle at the same spatial sampling by the solid line in blue, and the ideal model at full spatial sampling is represented by the “-.” curve in green.

Figure 6 shows the cumulative error between the phase of the sparsely sampled model, ϕ_u , and the measured phase ϕ'_u ,

$$\text{error}(x) = \sum_{u @ x=0 \text{ cm}}^{u @ x} |\phi_u - \phi'_u|, \quad (4)$$

where in the summation $u @ x = 0$ indicates the first pulse transmitted, and $u @ x$ indicates the pulse transmitted when the receiver is located at x , in reference to the abscissa in Figure 6. The cumulative error is also plotted for sub-bands of the same data in order to examine the effect of range resolution. Notice for the full 3.5 GHz bandwidth, the phase angle error increases slowly and uniformly until $x = 10$ cm where it

increases at a much faster rate. For the 1 GHz bandwidth, the distance where the cumulative error has a slow increase is shorter at approximately 3 cm. The 2 GHz bandwidth case has an immediate sharp increase, but the cumulative remains smaller than the 1 GHz bandwidth case after 3 cm. One reason for the this anomaly may be the spectrally dependent phase variation from this particular part of the reflecting surface.

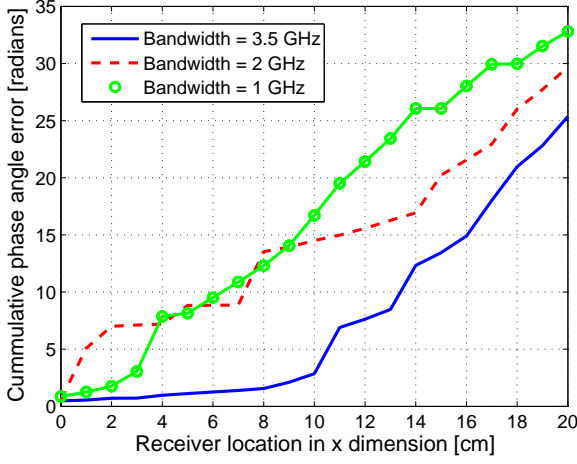


Fig. 6. Cumulative error in phase angle of the wall response for the full bandwidth in blue, and sub-bands in red and green.

Assuming for the moment that phase errors from moving the receiver assembly are minimal, the bistatic analysis in Figure 5 shows that coherent integration of the pulse compressed data from a moving target via multipath is reliable over the first 8 cm to 10 cm, in this case about 3λ . Thus, as a target traverses between the building and the radar, the response after standard Doppler processing (FFT) would be strongest where the phase variation matches the model well. From this observation, one may consider sacrificing SNR and Doppler resolution by using shorter CPIs when processing multipath, thus encouraging more reliable spatially coherent data. However, as mentioned before, other factors could be contributing to the phase error during this experiment, and the results are derived from one part of a wall of a particular building. Therefore, the analysis offers only a cursory examination of the multipath radar coherency issue and no broad conclusions can yet be drawn.

IV. MONOSTATIC MEASUREMENTS

The last portion of the experiment involved radar measurements of vehicles passing in front of the building. Two vehicle types were used, a 14 ft UHaul truck and a compact car, and both H pol and V pol data was collected. The transmit antennas from the bistatic measurements operated monostatically from the same transmit position in the far field of the wall indicated in Figure 1. The collections varied in vehicle speed (approximately 10 or 20 mph) and direction. With the radar close to the ground and by using an absorber fence to mitigate the ground bounce, we created a scenario similar to the two-dimensional analysis performed in [1]. We are able to validate

the geometric velocity and range predictions for the multipath responses, and lay the foundations of a model-based detection scheme that utilizes knowledge of the urban geometry assumes near-field integration of the wall reflection.

Figure 7 shows a range/Doppler image of the UHaul moving north at 8.94 m/s (in the $-x$ direction according to Figure 1) in front of the wall. The direct signal response, highlighted by the solid oval, is clearly noticeable and appears at the expected velocity according to the GPS coordinates that were recorded within the vehicle at the time and the static antenna location. The direct signal velocity response, v_{ds} , in relation to the angle of the incident field on the target is $v_{ds} = v_{tx} \cos \theta_i$, where v_{tx} is the speed of the truck in the x dimension.

Since the vehicles are in line-of-sight for this experiment, a “single-bounce” multipath response occurs where the transmit field is reflected from the wall and illuminates the target, which then scatters energy along a direct path back to the radar. The reciprocal path, where the field first scatters from the target to the wall and back to the radar, is also included. The single-bounce response for this collection is identified by the dashed-line oval in Figure 7. The single-bounce velocity is consistent with the predicted geometric model according to

$$v_{sb}(u, x_n) = v_{tx} [\cos \theta_i + \cos \theta_s(u, x_n)], \quad (5)$$

where $\theta_s(u, x_n)$ is the scattering angle between the wall and the target. The scattering point on the wall is represented by x_n , where n indexes the discrete sub-reflectors located along the length of the building. For double-bounce multipath, the transmitted field is reflected from the background wall to the target, which scatters energy back toward the wall and subsequently radiates in the direction of the radar. This multipath component is present when the target is in LOS and when it moves into the shadowed region. The predicted double-bounce velocity is

$$v_{db}(u, x_n) = \frac{v_{tx}}{2} [\cos \theta_s(u, x_n) + \cos \theta_s(u, x'_n)], \quad (6)$$

where x_n and x'_n are different sub-reflector locations on the wall. Note that eq. 6 does not depend on the radar location or the beam direction, but only on the scattering angles between the reflecting surface and the target. Scattering from subreflectors in the specular region will be stronger than other parts of the wall, however, so most of the double-bounce energy after pulse-Doppler processing indirectly depends on the incident beam angle. Given the known geometry and gps coordinates of the moving vehicle for this case, the predicted velocities are $v_{ds} = 6.5$ m/s, $v_{sb} = 6.0$ m/s, and $v_{db} = 5.5$ m/s, which are consistent with the responses in Figure 7.

We can also examine the power relation among the various signal components in Figure 7. Notice for the single-bounce multipath response, the attributes of power, shape and size are similar to those for the direct path response. For the double-bounce multipath, there is more than a 10 dB reduction in power for the range/Doppler cell of maximum strength in comparison with the direct and single-bounce responses. Furthermore, the spread of power among cells is much smaller for

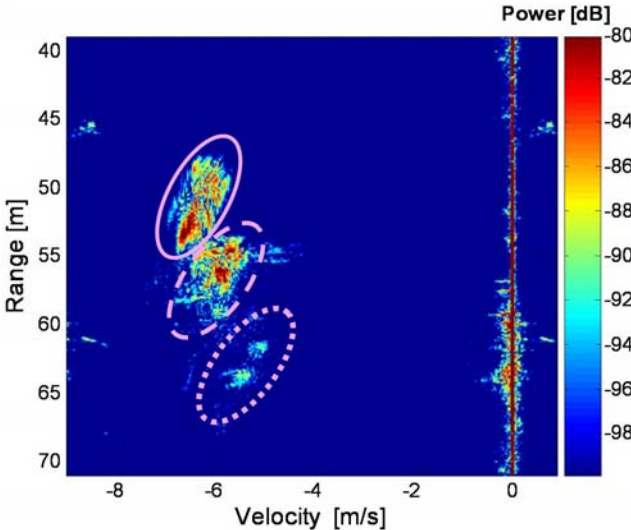


Fig. 7. Range/Doppler image (H pol) of the UHaul truck moving north, away from the radar (in the $-x$ direction) at approximately 20 mph (8.94 m/s). The direct signal response is identified by the solid oval. The single-bounce and double-bounce responses are indicated by the dashed and dotted ovals, respectively.

the double-bounce response, making detection using standard CFAR methods [3] of the non-LOS component challenging.

Figure 8 shows a range/Doppler image of the compact car moving north in front of the building at approximately 20 mph (GPS coordinates were not recorded for this vehicle so the instantaneous velocity correlated with the Figure is not verifiable and may be slightly faster than 20 mph). Note that the range of intensity values in this image had to be altered from those in Figure 7 in order to properly account for the target returns. The power of the LOS radar response for the car is almost 10dB weaker than the LOS power response of the UHaul truck. Moreover, the double bounce multipath response power is about 10 dB weaker than the LOS response from the car.

V. CONCLUSION

The motivation to perform the data collection described in this document was to gain knowledge of the electromagnetic phenomenology needed to develop GMTI radar techniques that exploit multipath in urban areas. Specifically, the bistatic collections yield information about a building reradiating energy on a target in the near-field. We showed that most of the power resided in the specular region of the range profile as expected, but the target would also be illuminated from other non-specular portions of the wall. This power could be utilized, via coherent or non-coherent integration, to assist in detecting targets given *a priori* knowledge of the urban geometry is available. We have also seen, for X-band radar, phase variations of the deramped fields reflected from the brick wall surface are fairly predictable. This is an encouraging assessment for reliable, coherent integration of multipath energy in terms of pulse compression. We also showed that the spatial correlation distance for coherent Doppler processing

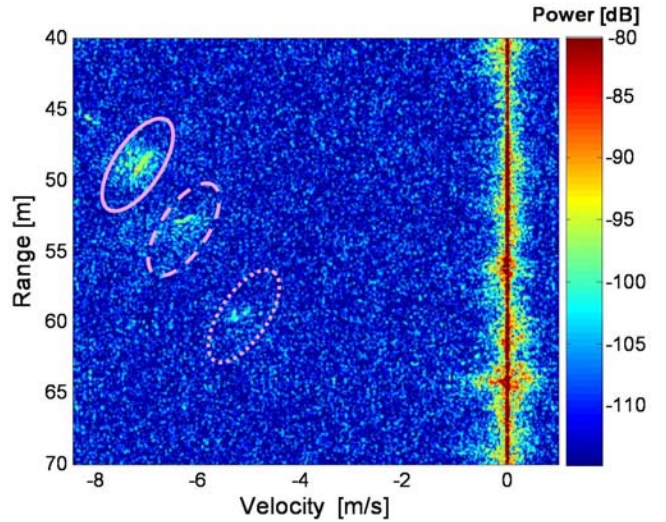


Fig. 8. Range/Doppler image (H pol) of the compact car moving north, away from the radar (in the $-x$ direction) at approximately 20 mph (8.94 m/s). The direct signal response is identified by the solid oval. The single-bounce and double-bounce responses are indicated by the dashed and dotted ovals, respectively.

of multipath radiation is only a few wavelengths (for the isolated case described in section III). Finally, the monostatic measurements of vehicles passing in front of the building allowed for pulse-Doppler processing to validate the direct and multipath predictions. These measurements have helped to characterize the reduction in power expected in the multipath return using standard GMTI processing, relative to the direct path return.

With further analysis, substantial conclusions can be garnered from this data and will be documented in future publications. Given the urban geometry is known *a priori*, a better understanding of the electromagnetic phenomenology may lead to model-based detection methods that exploit all available multipath energy.

ACKNOWLEDGMENT

The authors would like to thank Tom Caveyou, et al., from Matrix Research, Atindra Mitra from the RF Sensor Technology Division of the Air Force Research Laboratory/Sensor Directorate, and the Defense Advanced Research Projects Agency/Strategic Technology Office for their support.

REFERENCES

- [1] R.J. Linnehan, J.K. Schindler, "Multistatic scattering from moving targets in multipath environments," *Proc. IEEE Radar Conference*, May, 2009.
- [2] E.J. Baranoski, *Multipath Exploitation Radar Industry Day*, DARPA Strategic Technology Office Presentation, July, 2007.
- [3] M.A. Richards, *Fundamentals of Radar Signal Processing*, New York, NY: McGraw-Hill, 2005, pp. 347-363.